

CE74.55 Modeling of Water Resources Systems

February 24th and 25th, 2011

DISTRIBUTED RAINFALL-RUNOFF MODELING

Yasuto TACHIKAWA

Dept. of Civil and Earth Resources Eng., Kyoto University, Kyoto 615-8540, Japan
tachikawa@hywr.kuciv.kyoto-u.ac.jp

Modeling the actual hydrological response of a basin is a difficult task as the actual basin processes are complicated and basin properties change temporally as well as spatially. However, this difficulty can be addressed to some extent by using a distributed hydrological modeling approach, which is capable of incorporating the basin heterogeneity to model the basin hydrological responses. The paper introduces a basic idea of distributed hydrological modeling, which is organized as follows:

- Section 1 explains a basic concept of distributed hydrological modeling.
- Section 2 presents a typical water flow model embedded in a distributed hydrological model. As a flow model, the kinematic wave flow on a rectangular plane is explained.
- Section 3 explains numerical solution methods of the kinematic wave flow. A typical explicit method and an implicit method are introduced.
- Section 4 represents extensions of the kinematic wave model for surface and subsurface flow modeling.
- Section 5 shows applications of a distributed hydrologic model to basins with different catchment and climatic characteristics.
- Section 6 shows applications of a distributed hydrologic model for future discharge projection under climate change.

1 BASIC CONCEPT OF DISTRIBUTED HYDROLOGIC MODELING

1.1 Open-book type catchment modeling

A simple distributed hydrologic representation is a rainfall-runoff model based on an open-book catchment model. Figure 1 illustrates a schematic representation of an open-book catchment model. As its name implies, an open-book catchment model consists of two rectangular planes and a stream. Rain water flows on the planes and drains into the stream. The stream flow drains out of the catchment outlet. The flows on the rectangular planes and the stream are routed using a flow model such as the kinematic wave model. This is one of the simplest approximations of catchment hydrology using a distributed hydrologic model. A more complex structure of a catchment can be modeled as a cascade of the open-book catchment model as shown in Figure 2. Spatial distribution information of topography, soil characteristics, land cover and rainfall intensity are used for each sub-catchment.

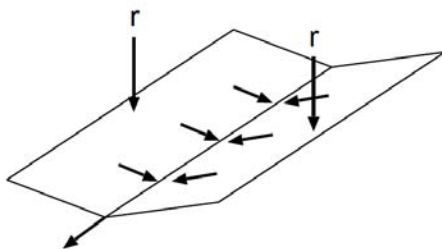


Figure 1: Schematic drawing of an open-book catchment model.

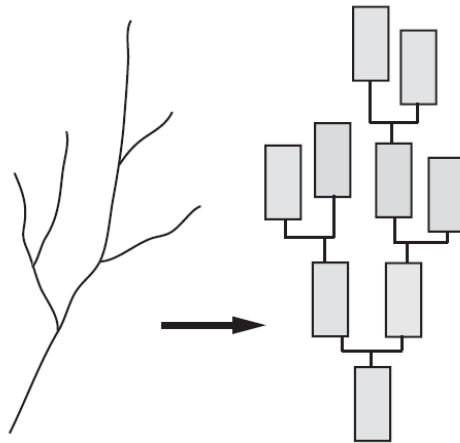


Figure 2: Cascade of the open-book catchment models.

1.2 Catchment modeling using Digital Elevation Models

Digital elevation models are now available at any catchments with a high spatial resolution enough to describe local catchment topography. For example, HydroSHED (Hydrological data and maps based on Shuttle Elevation Derivatives at multiple Scales, <http://hydrosheds.cr.usgs.gov/index.php>) provides hydrographic information for regional and global-scale, which includes digital elevations, drainage directions, and flow accumulation with the spatial resolutions of 3 arc-second (about 100m), 15 arc-second (about 500m) and 30 arc-second (about 1km). Figure 3 is an example of flow direction information derived from a grid-based DEM using the eight-direction method. After deriving the flow direction information, it is easy to define a rectangular plane formed by two adjacent grid points as shown in Figure 4. Catchment topography is represented by a set of slope units. For each slope unit, its area, length and gradient used for a flow model are easily calculated. A flow model such as the kinematic wave model is applied to all slope units and runoff is routed according to the flow direction information.

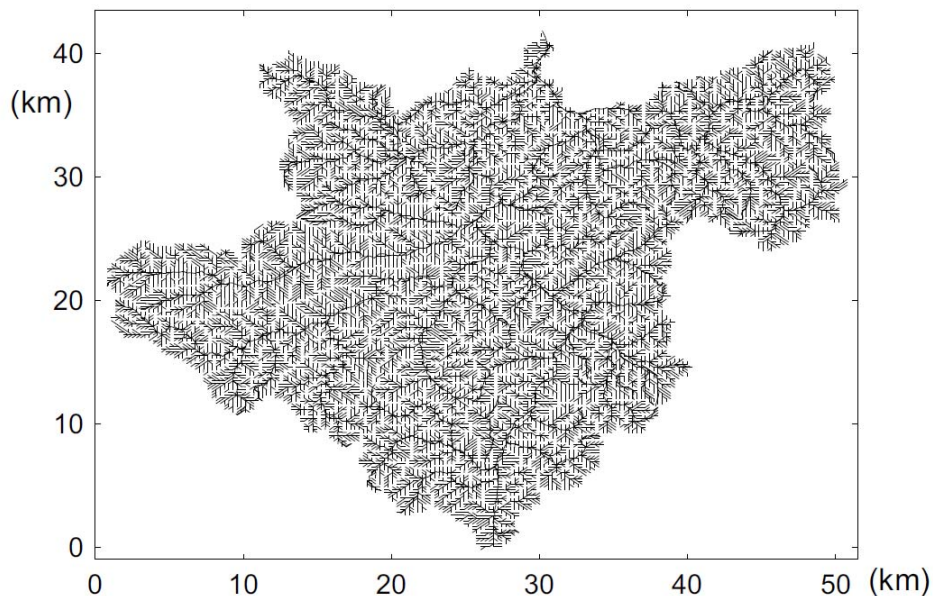


Figure 3: Flow direction information using a DEM at the Maruyama Basin in Japan.

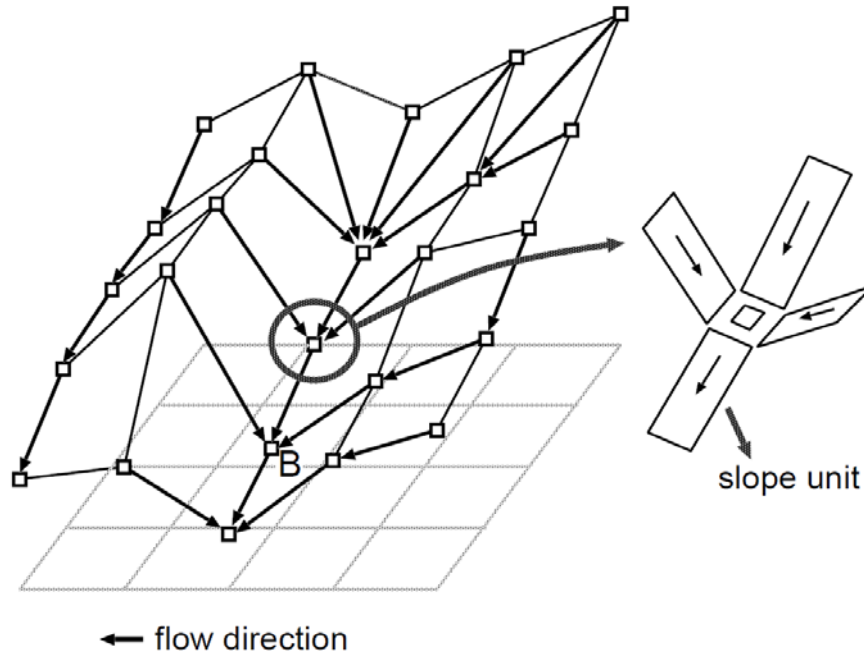


Figure 4: Schematic drawing of a catchment modelling using a DEM, which is a set of slope units connected according to the flow direction.

2 KINEMATIC WAVE MODEL

The kinematic wave model was originally developed for river routing. Then, it was applied to catchment rainfall-runoff modeling.

2.1 Basic theory

The basic form of the kinematic wave flow equation is:

$$\frac{\partial A}{\partial t} + \frac{\partial Q}{\partial x} = q_L(x, t) \quad (1)$$

$$Q = \alpha A^m \quad (2)$$

where $A(x, t)$ is the flow cross-sectional area, $Q(x, t)$ is the flow discharge, $q_L(x, t)$ is the lateral inflow per unit length and α and m are constants. Eq. (1) is the continuity equation and is derived from the principle of mass conservation within a control volume. Eq. (2) is derived from Manning's or Chezy's laws which are flow resistance laws of open channel uniform flow. Manning's law is described as:

$$v = \frac{1}{n} I^{1/2} R^{2/3} \quad (3)$$

in which v is the average flow velocity, n is the Manning's roughness coefficient, R is the hydraulic radius, and I is the friction slope. By assuming that R is expressed as $z_1 A^{z_2}$ (z_1 and z_2 are constants), we can easily obtain the expression of Eq. (2).

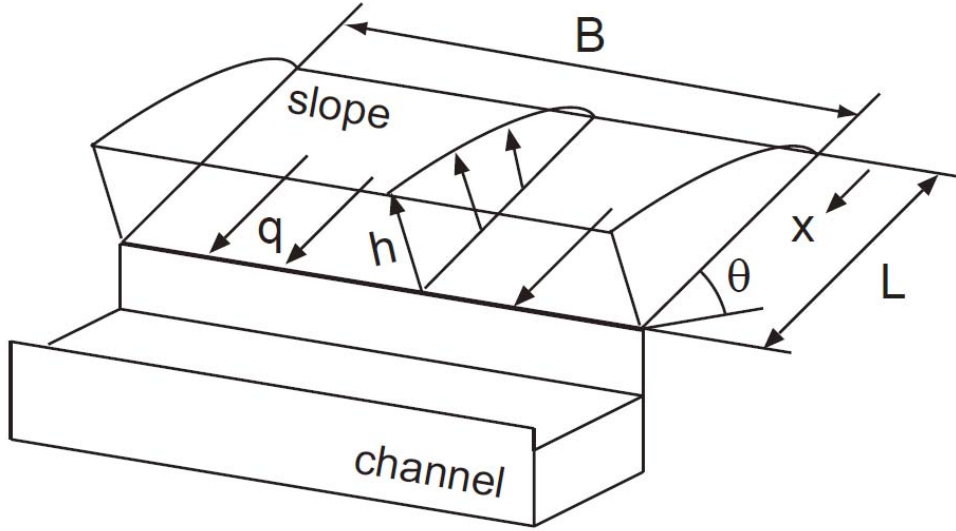


Figure 5: Shallow water flow on a rectangular plane.

2.2 Kinematic wave model for shallow surface flow on a rectangular plane

A catchment is often modeled as a rectangular plane or a set of rectangular planes as shown in Figure 2 and 4. The rainfall-runoff on a rectangle slope is modeled as a shallow water flow as shown in Figure 5. The hydraulic radius of shallow water flow can be approximated by the water depth h . Then, Eq. (3) is written as:

$$v = \frac{1}{n} I^{1/2} h^{2/3} \quad (4)$$

Then, discharge per unit width q is expressed as:

$$q = vh = \frac{1}{n} I^{1/2} h^{5/3} = \alpha h^m \quad (5)$$

in which $\alpha = \sqrt{I}/n$, $m = 5/3$. The value of I is usually approximated as the slope gradient of the rectangular plane, and the value of n is calibrated from observation or determined empirically. Eq. (5) is the momentum equation of the kinematic wave model on shallow water flow on a rectangular plane. The continuity equation becomes:

$$\frac{\partial h}{\partial t} + \frac{\partial q}{\partial x} = r = q_L / B \quad (6)$$

by dividing both sides of Eq. (1) with the width of a rectangular plane B , where r is rainfall intensity. Eqs. (5) and (6) are the basic equations of the kinematic wave model for shallow surface flow on a rectangular plane.

3 NUMERICAL SOLUTIONS OF KINEMATIC WAVE MODEL

The combination of Eqs. (5) and (6) derives a nonlinear first-order partial differential equation which describes the change of q and h in time and space. This equation can be solved by using numerical methods. Several methods are available, for example, the finite difference method, the finite element method, and the finite volume method. Here, the finite difference methods are introduced to solve the equation.

Finite difference methods are classified into two types, explicit and implicit methods. Explicit methods evaluate all spatial derivatives in a partial differential equation at the time level where the solution is known. Implicit methods evaluate all spatial derivatives at the time level where the solution is unknown. Generally, implicit methods are more complex than explicit methods; however the former is better in numerical stability to the latter.

3.1 Explicit method (The Lax-Wendroff scheme)

The Lax-Wendroff scheme is a typical explicit method to solve the kinematic wave flow numerically. Figure 6 shows the process to obtain the unknown variables defined at the grid points on discretized x - t plane. The subscripts i and j denote incremented time and space levels, respectively. This scheme calculates h_j^{i+1} from h_{j-1}^i , h_j^i , and h_{j+1}^i as stated below.

Expanding $h(x, t + \Delta t)$ using the Taylor's series up to the second order, we can obtain:

$$h(x, t + \Delta t) \simeq h(x, t) + \Delta t \frac{\partial h}{\partial t} + \frac{(\Delta t)^2}{2} \frac{\partial^2 h}{\partial t^2} \quad (7)$$

where Δt is the time step size. Eq. (6) can be rewritten as:

$$\frac{\partial h}{\partial t} = r - \frac{\partial q}{\partial x} \quad (8)$$

Using Eq. (8), $\partial^2 h / \partial t^2$ can also be rewritten as:

$$\begin{aligned} \frac{\partial^2 h}{\partial t^2} &= \frac{\partial}{\partial t} \left(\frac{\partial h}{\partial t} \right) \\ &= \frac{\partial}{\partial t} \left(r - \frac{\partial q}{\partial x} \right) \\ &= \frac{\partial r}{\partial t} - \frac{\partial}{\partial x} \left(\frac{\partial h}{\partial t} \frac{dq}{dh} \right) \\ &= \frac{\partial r}{\partial t} - \frac{\partial}{\partial x} \left\{ \left(r - \frac{\partial q}{\partial x} \right) \frac{dq}{dh} \right\} \end{aligned} \quad (9)$$

The right hand side of Eqs. (8) and (9) do not have derivatives of q and h with respect to time. We replace all derivatives in these expressions by difference operators as:

$$\frac{\partial h}{\partial t} \simeq r_j^i - \frac{q_{j+1}^i - q_{j-1}^i}{2\Delta x} \quad (10)$$

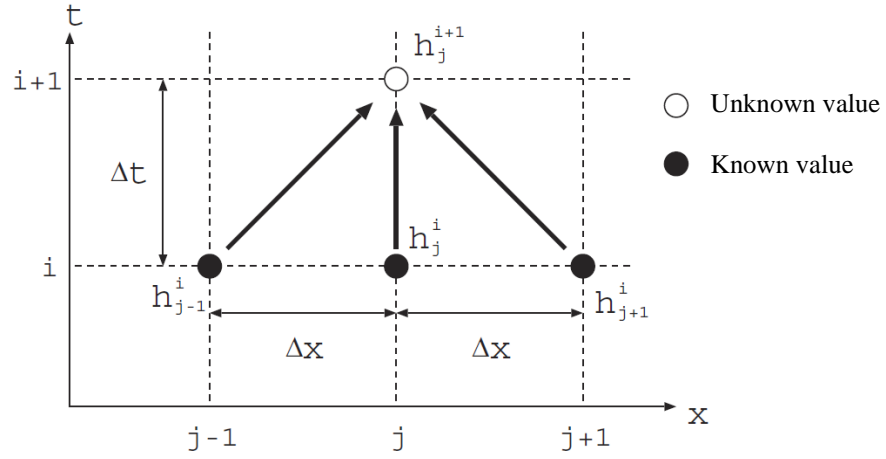


Figure 6: Schematic drawing of the Lax-Wendroff scheme on discretization of x - t plane.

$$\begin{aligned} \frac{\partial^2 h}{\partial t^2} \approx & \frac{r_j^{i+1} - r_j^i}{\Delta t} - \frac{1}{\Delta x} \left\{ \left(r_{j+1/2}^i - \frac{q_{j+1}^i - q_j^i}{\Delta x} \right) \times f' \left(\frac{h_{j+1}^i + h_j^i}{2} \right) \right. \\ & \left. - \left(r_{j-1/2}^i - \frac{q_j^i - q_{j-1}^i}{\Delta x} \right) \times f' \left(\frac{h_j^i + h_{j-1}^i}{2} \right) \right\} \end{aligned} \quad (11)$$

where Δx is the distance between two adjacent grid points, Δt is the time step size and $f' = dq/dh$. Let the right hand side of Eq. (10) be H_1 and that of Eq. (11) be H_2 , then we obtain:

$$h_j^{i+1} = h_j^i + \Delta t H_1 + \frac{(\Delta t)^2}{2} H_2 \quad (12)$$

This equation means h_j^{i+1} (and also q_j^{i+1}) can be calculated from h_{j-1}^i , h_j^i , and h_{j+1}^i as shown in Figure 6. For $j=n$, the following backward difference approximation:

$$h_n^{i+1} = h_n^i + \Delta t \left(r_n^i - \frac{q_n^i - q_{n-1}^i}{\Delta x} \right) \quad (13)$$

is used. When the upper boundary condition h_0^i , or q_0^i ($i = 0, 1, \dots$), and the initial conditions h_j^i or q_j^i , ($j = 0, 1, \dots, n$) are given, h_j^{i+1} can be calculated sequentially.

3.2 Implicit method (The four point implicit scheme)

The celerity of the kinematic wave is determined as:

$$c = \frac{dq}{dh} = f'(h) \quad (14)$$

By using Eq. (14), the continuity equation (6) can be rewritten as:

$$\frac{\partial q}{\partial t} + c \left(\frac{\partial q}{\partial x} - r \right) = 0 \quad (15)$$

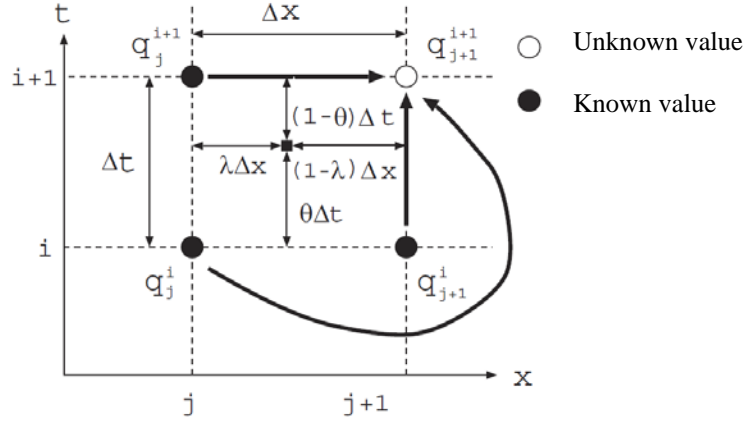


Figure 7: Schematic drawing of the four point implicit scheme on discretization of x - t plane.

Using the discretized x - t plane shown in Figure 7, each term of Eq. (15) can be written as:

$$\begin{aligned} \frac{\partial q}{\partial t} &\simeq (1 - \lambda) \frac{q_j^{i+1} - q_j^i}{\Delta t} + \lambda \frac{q_{j+1}^{i+1} - q_{j+1}^i}{\Delta t} \\ \frac{\partial q}{\partial x} &\simeq (1 - \theta) \frac{q_{j+1}^i - q_j^i}{\Delta x} + \theta \frac{q_{j+1}^{i+1} - q_j^{i+1}}{\Delta x} \end{aligned} \quad (16)$$

$$\begin{aligned} c &\simeq c_* = f' \left((1 - \theta) \{ \lambda h_{j+1}^i + (1 - \lambda) h_j^i \} + \theta \{ \lambda h_{j+1}^{i+1} + (1 - \lambda) h_j^{i+1} \} \right) \\ r &\simeq \bar{r} = \frac{1}{4} (r_j^i + r_{j+1}^i + r_j^{i+1} + r_{j+1}^{i+1}) \end{aligned} \quad (17)$$

in which Δx is the distance between two adjacent grid points, Δt is the time step size, θ is the time weighting parameter, and λ is the space weighting parameter. The default value of θ is 0.6 and λ is 0.5.

In Eq. (16), the unknown variable is q_{j+1}^{i+1} . Collecting unknown terms to the left hand side of the equation, we obtain:

$$q_{j+1}^{i+1} = \frac{\frac{\lambda}{\Delta t} q_{j+1}^i - \frac{1 - \lambda}{\Delta t} (q_j^{i+1} - q_j^i) + c_* \left\{ \frac{\theta}{\Delta x} q_j^{i+1} - \frac{1 - \theta}{\Delta x} (q_{j+1}^i - q_j^i) + \bar{r} \right\}}{\frac{\lambda}{\Delta t} + c_* \frac{\theta}{\Delta x}} \quad (18)$$

Eq. (18) is a nonlinear equation of q_{j+1}^{i+1} because c_* is dependent on the value of q_{j+1}^{i+1} . To solve the equation, an iterative method is used as follows:

step 1: Let the initial estimate of \hat{q}_{j+1}^{i+1} be $0.5(q_{j+1}^i + q_j^{i+1})$.

step 2: Obtain \hat{h}_{j+1}^{i+1} corresponding to \hat{q}_{j+1}^{i+1} .

step 3: Calculate c_* using Eq. (17).

step 4: Calculate an estimate of q_{j+1}^{i+1} using Eq. (18).

step 5: If $|q_{j+1}^{i+1} - \hat{q}_{j+1}^{i+1}| < \varepsilon$ (ε is a tolerance level), q_{j+1}^{i+1} is obtained. Otherwise, set q_{j+1}^{i+1} as a new estimated value \hat{q}_{j+1}^{i+1} and go back to the step 2.

4 KINEMATIC WAVE MODEL FOR SUBSURFACE FLOW

Several variations of the kinematic wave model were developed to improve the prediction accuracy of rainfall-runoff from catchments. These models realize various flow mechanisms, characteristics of soil and land use and these spatial distributions within a catchment.

4.1 Kinematic wave model for surface-subsurface saturated flow (Takasao & Shiiba, 1988)

The kinematic wave model described in 2.2 is applied to infiltration excess overland flow (Hortonian overland flow). To extend the discharge-depth relationship to represent saturation excess overland flow, Takasao and Shiiba (1988) developed a new discharge-depth relationship which includes both surface and subsurface flow and its interaction. They assumed that hillslope surface was covered by a soil layer with high surface infiltration capacity and permeability illustrated in Figure 8. In the figure, D is the depth of the soil layer, L is the length of the hillslope, H is the depth of water flow and r is the rainfall intensity. Let γ be the porosity of the soil layer and be spatially constant. Then the depth of the effective pore of the soil layer, d , becomes γD . Also, the actual water depth (water volume in height), h , becomes γH ($0 < H < D$) or $H - D + \gamma D$ ($H > D$). Takasao and Shiiba (1988) derived the following relation between h and q from Darcy's law and Manning's law:

$$q = \begin{cases} ah, & 0 \leq h \leq d \\ \alpha(h-d)^m + ah, & h \geq d \end{cases} \quad (19)$$

where $a = k \sin \theta / \gamma$ is the velocity of water which flows in the soil layer, k is the hydraulic conductivity, and $\alpha = \sqrt{\sin \theta} / n$ and $m = 5/3$, respectively. The upper relation given in Eq. (19) is used for the case where only subsurface flow occurs and the lower relation in Eq. (19) is used for the case where saturation excess overland flow occurs.

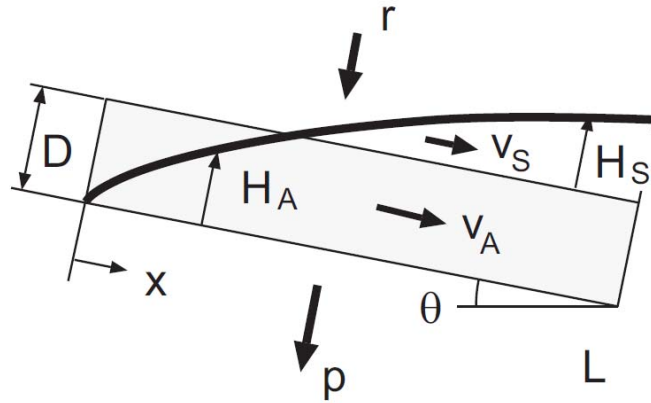


Figure 8: Schematic drawing of surface-subsurface flow on a hillslope.

4.2 Kinematic wave model for surface-subsurface saturated-unsaturated flow (Tachikawa et al., 2005)

The kinematic wave models described in 2.2 and 4.1 are basically used to simulate flood runoff which occurs in heavy rainfall events where the gravity force is dominant as a driving force of water flow. However these discharge-stage relations cannot be used in dry conditions because the capillary force of soil particles cannot be negligible in comparison with the gravity force in such conditions. To realize long term runoff simulations from dry to humid seasons continuously, Tachikawa et al. (2005) further extended the discharge-stage relation to realize both high flow and low flow simulation introducing an unsaturated flow mechanism in capillary pore of hillslope soil layer.

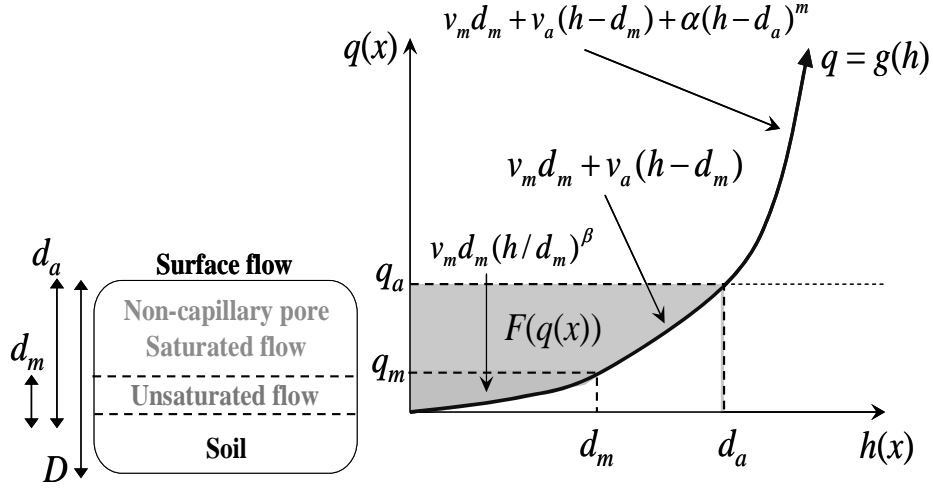


Figure 9: Schematic drawing of the discharge-depth relationship for saturated-unsaturated flow.

The discharge depth relation realizes three lateral flow mechanisms including 1) subsurface flow through capillary pore; 2) subsurface flow through non-capillary pore; and 3) surface flow on the soil layer (see Figure 9). At a slope segment, when the water depth is lower than the equivalent water depth for unsaturated flow ($0 < h < d_m$), flow is simulated by Darcy law with an unsaturated hydraulic conductivity k_m . If the water depth exceeds the equivalent depth for unsaturated flow, the exceeded water flows as saturated subsurface flow that is simulated by Darcy law with saturated hydraulic conductivity k_a . Once the water depth is greater than the effective soil layer $d_a = \gamma D$, the water flows as surface flow, which is simulated by the Manning's equation.

These three flow processes are represented by the following single set of stage-discharge relationship Eq. (20) and the continuity equation (6) (Tachikawa *et al.*, 2005; Sayama and McDonnel, 2009):

$$q = \begin{cases} v_m d_m (h/d_m)^\beta, & 0 \leq h \leq d_m \\ v_m d_m + v_a (h - d_m), & d_m \leq h \leq d_a \\ v_m d_m + v_a (h - d_m) + \alpha (h - d_a)^m, & d_a \leq h \end{cases} \quad (20)$$

$$v_m = k_m i, \quad v_a = k_a i, \quad k_m = k_a / \beta, \quad \alpha = \sqrt{i} / n$$

$$c^* = \frac{\partial q}{\partial h} = \begin{cases} \beta v_m (h/d_m)^{\beta-1}, & 0 \leq h \leq d_m \\ v_a, & d_m \leq h \leq d_a \\ v_a + m\alpha (h - d_a)^{m-1}, & d_a \leq h \end{cases} \quad (21)$$

where q is discharge per unit width, h is water depth, i is the slope gradient, k_m is the saturated hydraulic conductivity of the capillary soil layer, k_a is the hydraulic conductivity of the non-capillary soil layer, d_m is the depth of the capillary soil layer, d_a represents the depths of the capillary and non-capillary soil layers, β is the exponent constant of unsaturated flow, v_m and v_a are the flow velocities of unsaturated and saturated subsurface flows, respectively, and n is the Manning's roughness coefficient which varies as a function of land use type. Model parameters in the stage-discharge relationship are d_m , k_m , d_a , k_a , n , and $\beta (= k_a / k_m)$. The kinematic wave celerity for each layer is formulated in Eq. (21).

5 APPLICATION OF DISTRIBUTED MODEL

A distributed hydrologic model using the kinematic wave flow with the discharge-depth relationship (20) is applied to basins with different catchment and climatic characteristics.

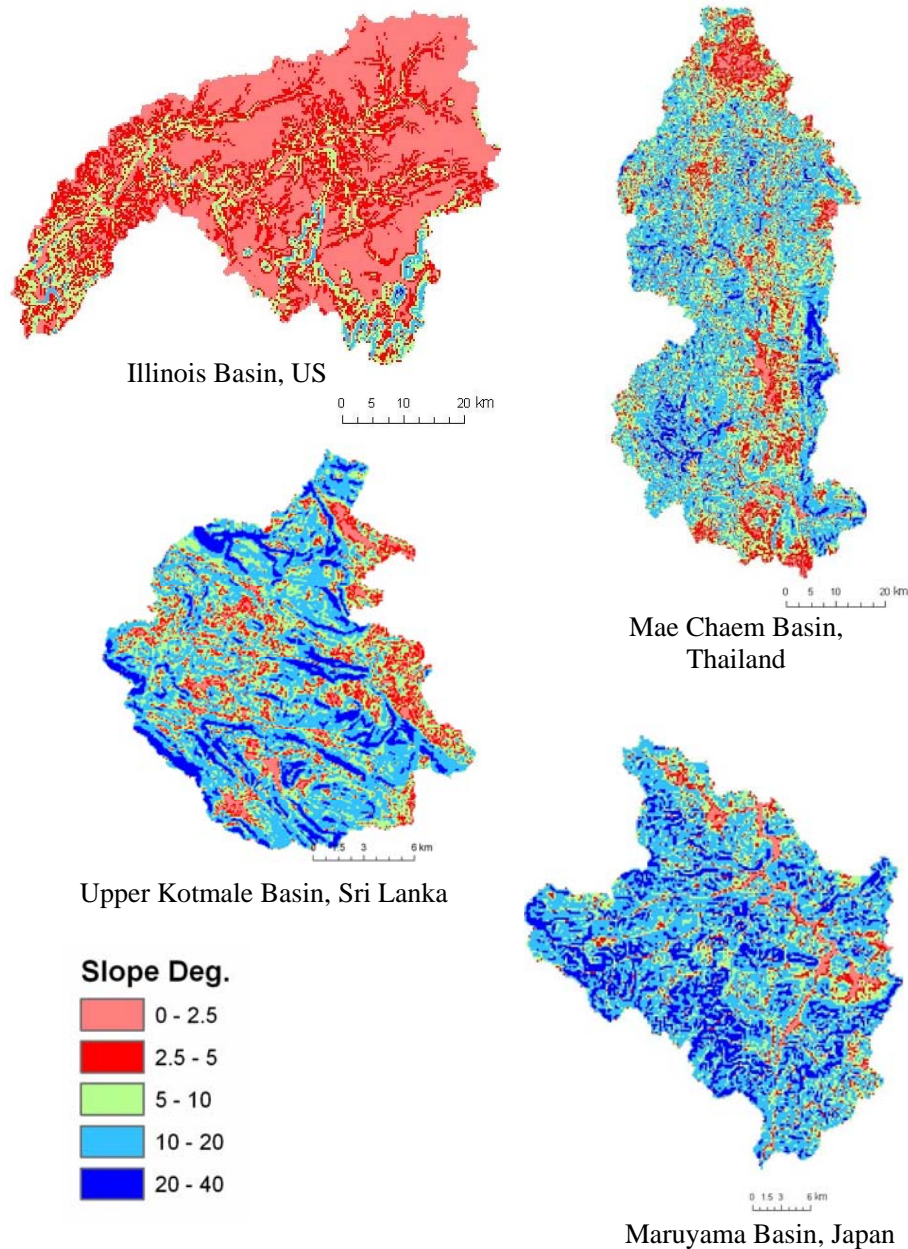


Figure 10: Study basins and slope distributions.

5.1 Simulation results at Maruyama basin in Japan

The Maruyama River basin is situated in the central part of Japan and the area of the basin is about 909 km². The catchment land use consist of 85% forest, 7 % rice, 2% buildings, 1% inland water and 5% others. The average annual rainfall of the basin is about 2,000 mm. Hourly flow data at the Fuichiba station for three flood events in 2004 and one event in 2003 are used in this study. Hourly rainfall data at ten stations within the Maruyama basin is also used. To represent the basin topography, the SRTM 90m digital

elevation model (USGS 2008, <http://seamless.usgs.gov/>) was used. Considering the computational time taken for automatic calibration of the distributed hydrological model, the original digital elevation model (DEM) was resampled to 250m grid size. The derived slope variation of the basin is shown in Figure 10.

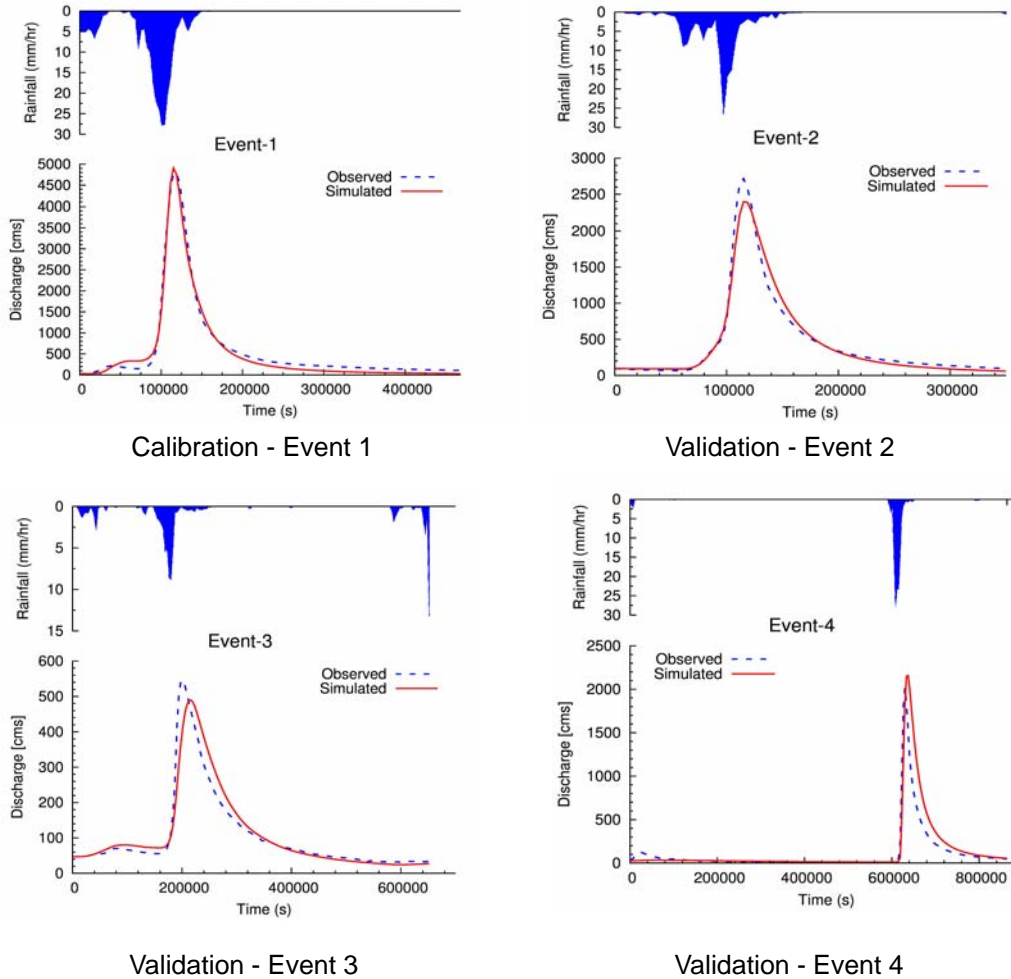


Figure 11: Observed and model predicted hydrographs for the Maruyama basin.

Figure 11 shows the observed and predicted flood hydrographs for the Maruyama basin for model calibration and validation. The distributed model is calibrated at the basin outlet for flood Event 1 using the SCE algorithm; then the calibrated model parameter set is used to predict the other flood events for validation. The hydrological model with the optimized parameter set for Event 1 predicted the peak flow and the time to peak of all flood events reasonably. To investigate further on these findings, the model was calibrated and validated for other three events independently. The model structure captures the governing hydrological processes in the steep and wet Maruyama basin.

5.2 Simulation results at the Upper Kotmale basin in Sri Lanka

The Upper Kotmale basin of 304 km² above the Thalawakelle station is the upper most basin of the Mahaweli River, one of the most important water resources in Sri Lanka. The terrain of the area is generally mountainous with moderate slope (Figure 10). The basin is situated in the wet zone of the country and the average annual rainfall varies from 2,200 mm to 2,600 mm. The catchment land use consists of tea 44%, forest 36%, home garden 7%, grass 5%, cash crops 5% and scrub. The main soil type

of the basin is silt loam. The Upper Kotmale basin was set up as an experimental basin in Sri Lanka for PUB studies and six tipping bucket rain gauges were installed in the basin. The data collection has been carried out since 2003 and we used hourly rainfall data for the study. Hourly flow data for two flood events from April to September, 2003 at the basin outlet Talawakelle is also used. The SRTM DEM of 90m was resampled to 250m grid size to represent the basin topography in the hydrological model.

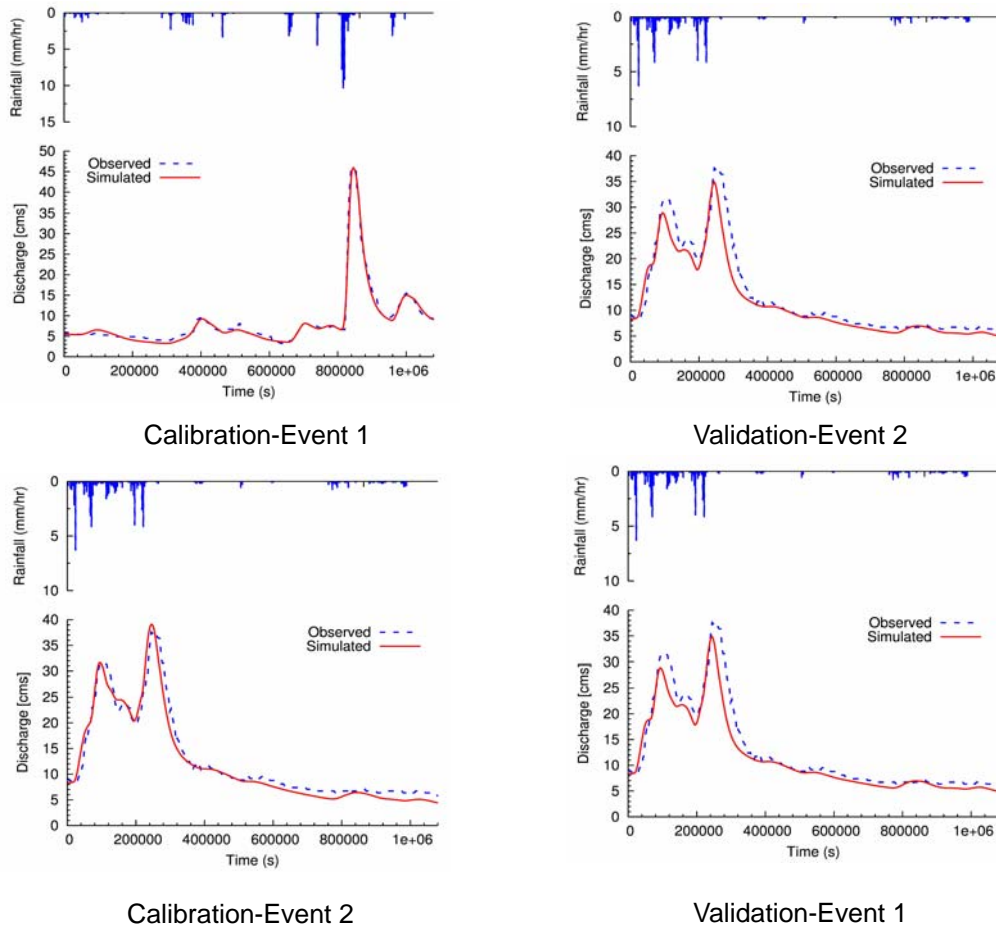


Figure 12: Observed and model predicted hydrographs of the Upper Kotmale basin.

Figure 12 shows the observed and predicted hydrographs for model calibration and validation. Two parameter sets are obtained for the basin by calibrating the model for each flood event independently using the SCE algorithm. Then the parameter set obtained for flood Event-1 was used to predict the flood Event-2 and vice-versa. The observed and predicted hydrographs for both events reasonably agreed with each other in the model calibration stage as well as in the model validation stage. The Nash coefficient value for both events in the model calibration is over 0.96 and the percentage error in the peak flow prediction is less than 4 %. Moreover, the percentage error in the flow volume is less than 10 % and also showed a high Nash coefficient value for both events in the model validation stage.

The model for the Upper Kotmale basin showed similar performances that we have experienced in Japanese basins. The identified values of the model parameters are different from Japanese basins, which would reflect the differences of land use and soil types. Wet and moderate slope basin or wet and steep slope basin tends to produce saturated subsurface flow and overland flow quickly after rainfall. The applied model structure fits to reproduce such quick response hydrological behaviors of these catchments. Only changing the model parameter values, the hydrological model reproduces hydrographs well in both calibration and validation. This suggests the model structure is transferable to these catchments.

6 APPLICATION OF DISTRIBUTED MODEL FOR RIVER FLOW PROJECTION UNDER CLIMATE CHANGE

Future river discharge projection was conducted using a distributed hydrologic model with a future climate projection data generated by the general circulation model (MRI-AGCM3.1S) developed by the Meteorological Research Institute in Japan. MRI-AGCM3.1S realizes 1920×960 of grid cells of about 20 km spatial resolutions (Kitoh et al., 2009). The products of MRI-AGCM3.1S consists of various atmospheric and hydrologic variables of the present climate experiment (1979-2003), the near future climate experiment (2015-2039), and the future climate experiment (2075-2099), which were simulated under the SRES A1B scenario.

The river discharge for the Chao Phraya River basins is predicted by feeding the future climate projection data into the 1km-spatial resolution distributed hydrologic model. The inputted data to the distributed hydrologic model as lateral flow is daily surface runoff generation and daily sub-surface runoff generation data, which are simulated by the land-surface process model embedded in the MRI-AGCM3.1S. Runoff simulation data of hourly maximum and daily mean are stored for each day with about 1km spatial resolution. The simulated discharge data were analyzed to discuss the change of the flood risk and water resources.

6.1 Change of floods

Annual maximum hourly discharge data was compiled and the statistical characteristics were analyzed. Figure 13(a) shows the change ratio of the mean of the annual maximum hourly discharge for the present climate experiment and the near future climate experiment. Generally, the annual maximum discharge of the main stream of the Chao Phraya River does not change, however the one of the tributaries changes location to location. Figure 13(b) shows the change ratio of the 10-year return period river discharge in the future climate experiment with respect to the future climate experiment using the Gumbel distribution. The spatial pattern is similar to the change of the mean of the annual maximum river discharge. It is important to recognize that the change of the discharge would appear especially at the tributaries.

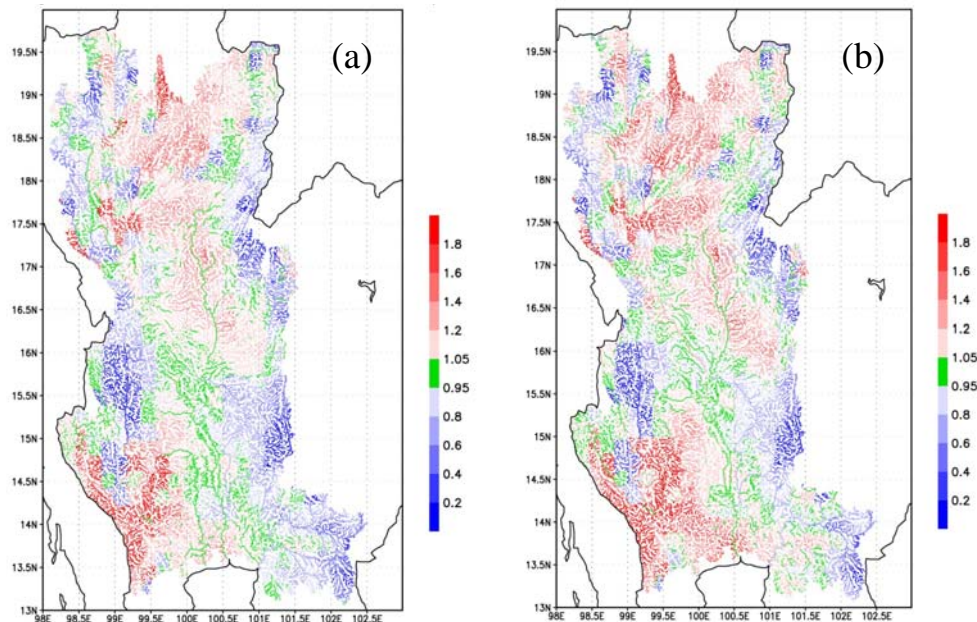


Figure 13: (a) Change of the ratio of the mean of the annual maximum hourly discharge in the future climate experiment with respect to the present climate experiment. (b) Change of the ratio of the 10-years return period river discharge in the future climate experiment with respect to the present climate experiment.

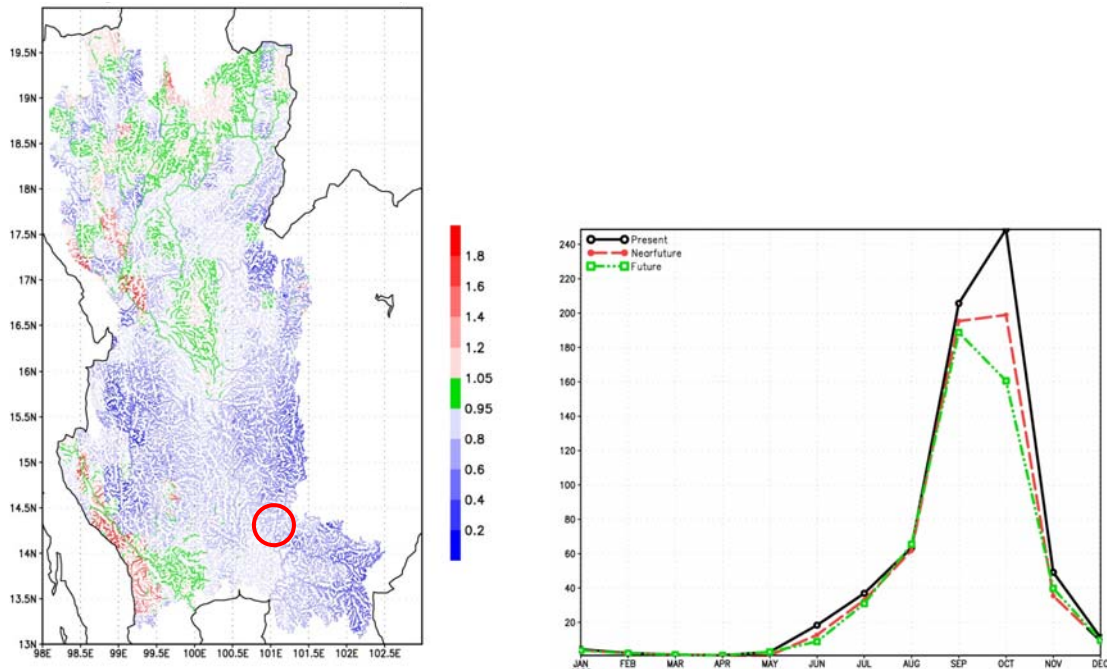


Figure 14: (a) Change of the ratio of the mean October discharge in the future climate experiment with respect to the present climate experiment. (b) Change of the monthly discharge at the lower reach of the Pasak River represented the circle in (a).

6.2 Change of water resources

Figure 14(a) shows the change ratio of the mean October discharge in the future climate experiment with respect to the present climate experiment. Generally, the monthly discharge on October decreases in the middle and lower part of the Chao Phraya River basin. Figure 14(b) shows the projected monthly discharge at the lower reach of the Pasak River. The figure shows the clear pattern of the decrease of the October discharge.

7 SUMMARY

Distributed hydrological modeling based on the kinematic wave flow was introduced. A distributed hydrologic model is capable of incorporating the basin heterogeneity to model the basin hydrological responses. The paper was organized as follows:

- Section 1 explains the basic concept of distributed hydrological modeling.
- Section 2 presents a water flow model embedded in a distributed hydrological model. As a typical flow model, the basic theory of the kinematic wave flow on a rectangular plane is explained.
- Section 3 explains numerical solution methods of the kinematic wave flow. A typical explicit method and an implicit method are introduced.
- Section 4 represents extensions of the kinematic wave model for surface and subsurface flow modeling.
- Section 5 shows applications of a distributed hydrological model to basins with different catchment and climatic characteristics.
- Section 6 shows applications of a distributed hydrologic model for future discharge projection under climate change.

REFERENCES

- Kitoh, A., Ose, T., Kurihara, K., Kusunoki, S., Sugi, M. and KAKUSHIN Team-3 Modeling Group (2009): Projection of changes in future weather extremes using super-high-resolution global and regional atmospheric models in the KAKUSHIN Program: Results of preliminary experiments, *Hydrological Research Letters*, Vol. 3, pp. 49-53.
- Sayama, T. and McDonnel, J. J. (2009) A new time-space accounting scheme to predict stream water residence time and hydrograph source components at the watershed scale, *Water Resources Research*, 45, pp. 1-14.
- Tachikawa Y., Nagatani, G. and Takara K. (2004) Development of stage-discharge relationship equation incorporating saturated-unsaturated flow mechanism, *Annual Journal of Hydraulic Engineering, JSCE*, 48, pp. 7-12 (in Japanese).
- Takasao T and Shiiba M. (1988) Incorporation of the effect of concentration of flow into the kinematic wave equations and its application to runoff system lumping, *Journal of Hydrology*, 102, pp. 301-322.

REFERENCES BOOKS

- Beven, K. J. (2000) *Rainfall-runoff Modeling The Primer*, Wiley.
- Bras, R. L. (1989) *Hydrology: An Introduction to Hydrologic Science*, Addison-Wesley.
- Brutsaert, W. (2005) *Hydrology: An Introduction*, Cambridge University Press.
- Chow, V. T., D. R. Maidment and L. W. Mays (1988) *Applied Hydrology*, McGraw-Hill.
- Eagleson, P. S. (1970) *Dynamic Hydrology*, McGraw-Hill.
- Hornberger, G. M., Raffensperger, J. P., Wiberg, P. L. and Eshleman, K. N. (1998) *Elements of Physical Hydrology*, The Johns Hopkins University Press.
- Maidment, D. R. (ed.) (1993) *Handbook of Hydrology*, McGraw-Hill.
- Vieux, B. E. (2004) *Distributed Hydrologic Modeling Using GIS*, second edition, Kluwer Academic Publishers.